Short form paper

Reorganization of nuclear pore complexes and lamina in late-stage parvovirus infection

Elina Mäntylä[1]#, Einari A. Niskanen[2], Teemu O. Ihalainen[3], and Maija Vihinen-Ranta[1]

[1]Department of Biological and Environmental Science and Nanoscience Center, University of Jyväskylä, Jyväskylä, Finland

[2]Institute of Biomedicine, University of Eastern Finland, Kuopio, Finland

[3]NeuroGroup, BioMediTech, University of Tampere, Tampere, Finland

Key words: Late-infection, canine parvovirus, change in nuclear architecture, nuclear pore complex, nuclear lamina, apical side of the nucleus

Running title: Parvovirus induced changes in nuclear organization

#Address correspondence to Maija Vihinen-Ranta, maija.vihinen-ranta@jyu.fi

University of Jyväskylä, Department of Biological and Environmental sciences, P.O. Box 35, FI-40014 University of Jyväskylä, Finland. Phone: +358 400 248 118

Abstract word count: 75 Text word count: 1643

Abstract

Canine parvovirus (CPV) infection induces reorganization of nuclear structures. Our studies indicated that late-stage infection induces accumulation of nuclear pore complexes (NPCs) and lamin B1 concomitantly with decrease of lamin A/C on the apical side of the nucleus. Newly formed CPV capsids are located in close proximity of NPCs on the apical side. These results suggest that parvoviruses cause apical enrichment of NPCs and reorganization of nuclear lamina presumably to facilitate the late-stage infection.

Journal of Virology JVI Journal of Virology

Text

Nuclear lamina is a protein-rich structural scaffold, the main components of which are the dynamic type V intermediate filament proteins called lamins. Lamin proteins comprise two subtypes, type A (lamin A, A10, C and C2) and type B (B1, B2 and B3). The former are alternative splice products of *LMNA* gene, and the latter are encoded by *LMNB1* (B1) and *LMNB2* (B2 and germ line specific B3) genes, respectively (1). In structure the lamins of both subtypes contain a central α-helical rod with a globular head (N-) and tail (C-) domains. *In vitro*, the lamins dimerize in a parallel fashion followed by filament assembly (2,3). The lamina is connected to the cytoskeleton via the nuclear envelope (NE) spanning linker of nucleoskeleton and cytoskeleton (LINC) –complex (4). Lamina also interacts with nuclear pore complexes (NPCs) consisting of ~30 nucleoporins (Nups) and regulating bidirectional transport of molecules over the NE (5). Together, the NPCs and lamina define a dynamic barrier that mediates signals in response to cellular stress conditions such as virus infections and limits release of viral progeny after nuclear assembly (6-9). To overcome this, viruses are known to alter the architecture of all aforementioned subnuclear structures which in turn contribute to the function of the nucleus (10). Nuclear egress of parvovirus capsids has been suggested to occur by active export via the NPC pathway prior to cell lysis (11-13). However, the influence of parvovirus egress on the organization of NPCs and nuclear lamina is unknown. Here, we examined the distribution and organization of NPCs as well as A and B type lamins in canine parvovirus (CPV) infected cells in late infection in comparison with those in non-infected S- and G-phase (G1/G2) cells.

The NPCs are dynamic structures capable of assembly, disassembly and redistribution during the cell cycle (14,15). The nucleus has a spatially polarized architecture (16), however, the NPC distributions between the apical and basal sides of the nucleus have not been comparatively determined. Here, we examined the spatial distributions of NPCs at the apical and basal sides of nuclei in CPV infected (MOI 1; at 24 h post infection, p.i.) and mock-infected S- or G1/G2 – phase Norden laboratory feline kidney (NLFK) cells. The NPCs were immunostained with a nucleoporin 153 (Nup153) antibody (Ab) (ab24700-Abcam, Cambridge, UK) also recognizing Nup62. A proliferating cell nuclear antigen (PCNA) Ab (ab18197, Abcam, Cambridge, UK) was used as a marker for cell cycle phases and the presence of parvoviral replication body (17,18) (Fig. 1A). In confocal microscopy, z-stacks consisting of average 30 z-plains spaced by 0.15 µm were collected with the z-axis corresponding to the apical–basal axis of cell nucleus. Nuclei were scanned over a range of 4 to 6 µm. Middle z-plain was applied to define the position of basal and apical surfaces. Confocal microscopy of infected cells showed unequal distribution of NPCs on the apical and the basal side of NE. Firstly, the number of NPCs at the apical side was ~31 % higher than that at the basal side (Fig. 1B). In G1/G2 cells the distribution of NPCs was also asymmetric with ~20 % more NPCs at the apical than the basal side. In the S-phase NPCs were more equally distributed with only ~10 % more NPCs localized to the apical side. Secondly, the overall NPC density on both the apical and basal sides was significantly decreased in infection (Fig. 1C). In the infected cells, the apical NPC density (number of NPCs/µm^2 ± SD, 3.6 ± 0.51 NPC/µm^2, n=22) was lower than in the S- (4.0 ± 0.42 NPC/µm^2, n=21, Student´s t-test $p<0.05$) or G-phase control cells (4.12 ± 0.48 NPC/µm^2, n=22, $p<0.01$) (Fig. 1A and 1C). Even more prominent decrease was seen at the basal side of infected cell nuclei, where NPC density (2.51 ± 0.65 NPC/ µm^2, n=22) was ~25% lower than in the mock-infected G-phase (G1/G2) cells, and

~30% lower than in S-phase cells (3.36 ± 0.88, n=21, $p<0.01$; 3.57 ± 0.31 NPC/μm^2, n=22, $p<0.01$, respectively) (Fig. 1A and C). Our results showed that infection was accompanied by a profound modification of the NPC network including significant reduction in the density of NPCs at the basal side, resembling the overall NPC distribution in G1/G2 cells. Earlier studies have shown that cell cycle dependent increase in the amount of NPCs and nuclear volume occur simultaneously; however, with different regulation mechanisms (15,19). The frequency of NPC biogenesis fluctuates during cell cycle progression being highest in S and G_2 phases (19-21). CPV infection is accompanied by cell cycle arrest into S phase (22-24). Notably, in contrast with the high density of NPCs seen in S-phase cells, we observed significantly decreased density in infected cells. To exclude that the decrease in NPC density was due to infection-induced degradation, the structural integrity of Nup153 in the infected cells at 24 h p.i was analyzed by Western blot (4.2 x 10^4 cells per well). The analysis of FG-repeated Nup153 and Nup62 (Nup153 Ab; Mab414, ab24609, Abcam) in infected and mock-infected cells showed no major difference in abundance or integrity (Fig. 1D). For comparison, actinomycin D (Act D) treated (0.5-1 µg/ml, 24 h) apoptotic cells showed cleavage of Nup153 (data not shown). However, in the infected cells two additional bands with lower electrophoretic mobility was seen. The change may reflect post-translational modification of Nup153 such as increased phosphorylation. With many viruses, Nup153 undergoes structural modification to support viral replication and spread. As an example, viruses use phosphorylation of Nups to alter nucleocytoplasmic transport of the host (25). Furthermore, phosphorylation of Nups can occur in response to DNA damage, commonly detected in parvovirus infections (26,27), and indicate an infection-induced functional change of Nup153 (28,29). Our analyses do not exclude the possibility of Nup153 becoming detached from the NPCs in infection. However, the amount of homogenously distributed Nup153

96 in the cytoplasm seemed to remain unaltered as judged by confocal microscopy (Fig. 1A). Taken
97 together, these results demonstrated that CPV infection is accompanied by accumulation of
98 NPCs at the apical side of the nucleus along with a decrease in their overall density
99 concomitantly with structural modification of Nup153.

100 NPCs are anchored into the nuclear lamina (30,31). B-type lamins concentrate in pore-rich
101 regions whereas A-type lamins are found in pore-free islands (32). Accordingly, changes in the
102 distribution of NPCs correlate with nuclear lamina reorganization (19,33). As CPV infection was
103 accompanied by significant changes in the distribution of NPCs, we next analyzed the
104 distributions of lamins at apical and basal sides of the nucleus. Immunofluorescence analysis was
105 carried out with antibodies recognizing lamins A/C and B1 (NCL-LAM-A/C, monoclonal, Leica
106 Biosystems, Newcastle, UK; ab16048, polyclonal, Abcam, Cambridge, UK). In virus-infected
107 cells, similarly to NPCs, lamin B1 was enriched in clusters along the apical side of the NE (Fig.
108 2A), whereas in mock-infected cells lamin B1 was distributed more equally between the two
109 sides. These data suggested that infection affected the composition of lamina or lamin epitope.
110 To study the distributions of lamins A/C and B1 in more detail, we first compared their
111 intensities at the apical and basal sides (n=24) (Fig. 2B) and then obtained surface intensity ratios
112 (apical intensity divided by basal intensity) for both lamins (n=24) (Fig. 2C). At the apical side
113 of mock-infected cells, the intensity of lamin AC was ~16 % higher than that of lamin B1. In
114 infection, the intensity of lamin A/C at the apical side was significantly ($p<0.05$) decreased and
115 was ~6 % lower than that of lamin B1 (Fig. 2B). At the basal side, the average intensities of both
116 lamins were significantly ($p<0.05$) decreased in infection in comparison with those in mock-
117 infected cells. Determination of surface intensity ratios showed that in general, lamin intensities
118 were higher at the apical side than the basal side (Fig. 2C) as reported earlier (16). In infection,

the surface intensity ratio of lamin B1 was slightly increased while that of lamin A/C was similar in comparison with those in the mock-infected cells (Fig. 2C). These results showed that infection was accompanied by a decrease in the abundance of lamin A/C in the lamina concomitantly with enrichment of lamin B1 at the apical side. We then analyzed if the infection-induced changes in distributions of lamins were due to their degradation. Western blot analysis (4.2×10^4 cells per well) indicated that lamins A/C and B1 (ab8984; ab16048, Abcam, Cambridge, UK) remained intact in infection (Fig. 3A), but disintegrated in Act D-induced (1 and 5 μg/ml, 24 h) apoptotic cells (Fig. 3B). This agrees with earlier data showing that parvoviral nuclear egress does not induce degradation of lamins (34). Importantly, the expression levels of lamin A/C and B1 in the infected and mock-infected cells were comparable (Fig. 3A). In parallel, confocal imaging showed no marked discontinuity in lamin A/C or B1 staining in the infected cells i.e. lamin A/C and lamin B1 layers remained continuous even when viral capsids accumulated in the nuclear periphery at late-stage infection (Fig. 3C). Finally, the apical distributions of lamin B1, Nup153 and newly formed CPV capsids were compared in infection from deconvoluted confocal YZ cross-sections and analyzed with the program ImageJ. Apical distribution of lamin B1 was found to be similar with that of Nup153 (Fig. 4A, 4B and 4C) and virus capsids (Fig. 4D, 4E and 4F). Importantly, virus capsids were concentrated beneath apical NPCs (Fig. 4G, 4H and 4I). In summary, our results indicated that in CPV infection lamin B1 was enriched in the apical side concomitantly with overall decrease of lamin A/C. Instead of inducing degradation, parvovirus infection might influence the organizational and/or functional status of nuclear lamins.

To conclude, we observed that in late-stage parvovirus infection significant relocation of NPCs and reorganization of nuclear lamina occurred at the apical side of the nucleus. These changes

were associated with the location of viral capsids in close proximity to apical NPCs. These results suggest that reorganization of nuclear envelope might be important for viral egress. This study extends knowledge on parvovirus nuclear egress and accompanying virus-induced changes in organization of the NPCs and the nuclear lamina.

Acknowledgements

We thank Colin Parrish for the infectious CPV clone and CPV antibodies. We are grateful to Klaus Hedman for comments on the manuscript. This work was financed by the Academy of Finland under the award numbers 135609 (EAN), 267471 (TOI) and 138388 (MVR).

References:

1. **Dittmer TA, Misteli T.** 2011. The lamin protein family. Genome Biol **12:**222-222. doi: 10.1186/gb-2011-12-5-222.

2. **Gruenbaum Y, Medalia O.** 2015. Lamins: the structure and protein complexes. Curr Opin Cell Biol **32:**7-12. doi:10.1016/j.ceb.2014.09.009.

3. **Köster S, Weitz DA, Goldman RD, Aebi U, Herrmann, H.** 2015. Intermediate filament mechanics in vitro and in the cell: from coiled coils to filaments, fibers and networks. Curr Opin Cell Biol **32:**82-91. doi: 10.1016/j.ceb.2015.01.001.

4. **Ho CY, Lammerding J.** 2012. Lamins at a glance. J Cell Sci **125:**2087-2093. doi: 10.1242/jcs.087288.

5. **Fahrenkrog B, Köser J, Aebi U.** 2004. The nuclear pore complex: a jack of all trades? Trends Biochem Sci **29:**175-182. doi: 10.1016/j.tibs.2004.02.006.

6. **Osmanagic-Myers S, Dechat T, Foisner R.** 2015. Lamins at the crossroads of mechanosignaling. Genes Dev **29:**225-237. doi: 10.1101/gad.255968.114.

7. **Pascual-Garcia P, Capelson M.** 2014. Nuclear pores as versatile platforms for gene regulation. Curr Opin Genet Dev **25:**110-117. doi: 10.1016/j.gde.2013.12.009.

8. **Cibulka J, Fraiberk M, Forstova J.** 2012. Nuclear actin and lamins in viral infections. Viruses **4:**325-347. doi: 10.3390/v4030325.

9. **Malhas AN, Lee CF, Vaux DJ.** 2009. Lamin B1 controls oxidative stress responses via Oct-1. J Cell Biol **184:**45-55. doi: 10.1083/jcb.200804155.

10. **Zakaryan H, Stamminger T.** 2011. Nuclear remodelling during viral infections. Cell Microbiol **13:**806-813. doi: 10.1111/j.1462-5822.2011.01596.x.

11. **Cotmore SF, Tattersall P.** 2014. Parvoviruses: small does not mean simple. Annu Rev Virol **1:**517-537. doi: 10.1146/annurev-virology-031413-085444.

12. **Engelsma DN, Valle N, Fish A, Salomé N, Almendral JM, Fornerod M.** 2008. A supraphysiological nuclear export signal is required for parvovirus nuclear export. Mol Biol Cell **19:**2544-2552. doi: 10.1091/mbc.E08-01-0009.

13. **Maroto B, Valle N, Saffrich R, Almendral JM.** 2004. Nuclear export of the nonenveloped parvovirus virion is directed by an unordered protein signal exposed on the capsid surface. J Virol **78:**10685-10694. doi: 10.1128/JVI.78.19.10685-10694.2004.

14. **Imamoto N, Funakoshi T.** 2012. Nuclear pore dynamics during the cell cycle. Curr Opin Cell Biol **24:**453-459. doi: 10.1016/j.ceb.2012.06.004.

15. **Dultz E, Ellenberg J.** 2010. Live imaging of single nuclear pores reveals unique assembly kinetics and mechanism in interphase. J Cell Biol **191:**15-22. doi: 10.1083/jcb.201007076.

16. **Kim D, Wirtz D.** 2015. Cytoskeletal tension induces the polarized architecture of the nucleus. Biomaterials. 48:161-172. doi: 10.1016/j.biomaterials.2015.01.023.

17. **Essers J, Theil AF, Baldeyron C, van Cappellen WA, Houtsmuller AB, Kanaar R, Vermeulen W.** 2005. Nuclear dynamics of PCNA in DNA replication and repair. Mol Cell Biol **25:**9350-9359. doi: 10.1128/MCB.25.21.9350-9359.2005.

18. **Ihalainen TO, Niskanen EA, Jylhävä J, Paloheimo O, Dross N, Smolander H, Langowski J, Timonen J, Vihinen-Ranta M.** 2009. Parvovirus induced alterations in nuclear architecture and dynamics. Plos One. **4:**e5948.

19. **Maeshima K, Iino H, Hihara S, Funakoshi T, Watanabe A, Nishimura M, Nakatomi R, Yahata K, Imamoto F, Hashikawa T, Yokota H, Imamoto N.** 2010. Nuclear pore formation

but not nuclear growth is governed by cyclin-dependent kinases (Cdks) during interphase. Nat Struct Mol Biol **17:**1065-1071.

20. **Maul GG, Maul HM, Scogna JE, Lieberman MW, Stein GS, Hsu BY, Borun TW.** 1972. Time sequence of nuclear pore formation in phytohemagglutinin-stimulated lymphocytes and in HeLa cells during the cell cycle. J Cell Biol **55:**433-447. doi: 10.1083/jcb.55.2.433.

21. **Winey M, Yarar D, Giddings TH, Mastronarde DN.** 1997. Nuclear Pore complex number and distribution throughout the Saccharomyces cerevisiae cell cycle by three-dimensional reconstruction from electron micrographs of nuclear envelopes. Mol Biol Cell **8:**2119-2132.

22. **Nykky J, Tuusa JE, Kirjavainen S, Vuento M, Gilbert L.** 2010. Mechanisms of cell death in canine parvovirus-infected cells provide intuitive insights to developing nanotools for medicine. Int J Nanomedicine **5:**417-428.

23. **Rothballer A, Kutay U.** 2013. Poring over pores: nuclear pore complex insertion into the nuclear envelope. Trends Biochem Sci **38:**292-301. doi: 10.1016/j.tibs.2013.04.001.

24. **Antonin W, Ellenberg J, and Dultz E.** 2008. Nuclear pore complex assembly through the cell cycle: Regulation and membrane organization. FEBS Lett **582:**2004-2016. doi: 10.1016/j.febslet.2008.02.067.

25. **Porter FW, Palmenberg AC.** 2009. Leader-induced phosphorylation of nucleoporins correlates with nuclear trafficking inhibition by cardioviruses. J Virol **83:**1941-1951. doi: 10.1128/JVI.01752-08.

26. **Cotmore SF, Tattersall P.** 2013. Parvovirus diversity and DNA damage responses. Cold Spring Harb Perspect Biol **5:**a012989. doi: 10.1101/cshperspect.a012989.

27. **Luo Y, Qiu J.** 2013. Parvovirus infection-induced DNA damage response. Future Virol **8:**245-257. doi: 10.2217/fvl.13.5.

28. **Güttinger S, Laurell E, Kutay U.** 2009. Orchestrating nuclear envelope disassembly and reassembly during mitosis. Nat Rev Mol Cell Biol **10:**178-191.

29. **Wan, G, Zhang X, Langley RR, Liu Y, Hu X, Han C, Peng G, Ellis LM, Jones SN, Lu X.** 2013. DNA damage-induced nuclear export of precursor microRNAs is regulated by the ATM-AKT pathway. Cell Rep **3:**2100-2112. doi: 10.1016/j.celrep.2013.05.038.

30. **Hutchison CJ.** 2002. Lamins: building blocks or regulators of gene expression? Nat Rev Mol Cell Biol **3:**848-858.

31. **Guo Y, Kim Y, Shimi T, Goldman RD, Zheng Y.** 2014. Concentration-dependent lamin assembly and its roles in the localization of other nuclear proteins. Mol Biol Cell **25:**1287-1297. doi: 10.1091/mbc.E13-11-0644.

32. **Maeshima K, Yahata K, Sasaki Y, Nakatomi R, Tachibana T, Hashikawa T, Imamoto F, Imamoto N.** 2006. Cell-cycle-dependent dynamics of nuclear pores: pore-free islands and lamins. J Cell Sci **119:**4442-4451. doi: 10.1242/jcs.03207.

33. **Fiserova J, Goldberg M.** 2010. Relationships at the nuclear envelope: lamins and nuclear pore complexes in animals and plants. Biochem Soc Trans **38:**829.

34. **Nüesch JPF, Lachmann S, Rommelaere J.** 2005. Selective alterations of the host cell architecture upon infection with parvovirus minute virus of mice. Virology **331:**159-174. doi: 10.1016/j.virol.2004.10.019.

Figure legends:

Figure 1. Infection and cell cycle dependent distribution of nuclear pore complexes. (A) Confocal microscopy images of the infected cells at 24 h p.i. and the mock-infected cells in S and G1/G2 –phases. NPCs and PCNA were visualized with Nup153 (left and middle panel) and PCNA (right panel) antibodies. (B) The amount of NPCs calculated from the apical and basal sides of NE. (C) Average density of NPCs in apical and basal side of NE. The average values of triplicates with ±SD are shown. (D) Western blot analysis of Nup153 and Nup62 proteins and their structural integrity harvested from the infected and mock-infected cells. Nups were detected with Nup153 specific antibody and Mab414 antibody recognizing FG-repeated Nup62 and Nup153 in feline cells. Scale bars, 10 µm. Error bars represent the 95 % confidence interval.

Figure 2. Distributions of lamin A/C and lamin B1. (A) Confocal yx and yz cross-sections taken through the nucleus show localization of lamin A/C (green) and lamin B1 (red) Abs in mock-infected (left) and infected (right) cells. Arrowheads show lamin B1-enriched areas. (B) Average intensities of lamin A/C and B in apical and basal sides of NE. (C) Surface intensity ratio between apical and basal side for both lamins individually by ImageJ. Error bars represent the 95% confidence intervals. Statistical significance in comparison to the mock-infected cells is shown (Student´s T-test p-values: *P<0.05;**P< 0.01). Scale bars, 10 µm.

Figure 3. Structural integrity of lamins. (A) Western blot analysis of structural integrity of lamins A/C and B1 in infected, mock-infected and (B) actinomycin D (1-5 µg/ml) treated cells.

Asterisks indicate disintegration products of lamins. (C) Confocal microscopy sections of infected cells showing distribution of lamin A/C, lamin B1 and accumulation of viral capsids to the nuclear periphery at 24 p.i. Scale bar, 5 µm.

Figure 4. Intranuclear localization of lamin B1, NPCs and viral capsids. Confocal microscopy derived apical max intensity projections with yz cross-sections showing intranuclear distribution of (A,B) NPCs (red) and lamin B1 (green), (D,F) virus capsids (red) and lamin B1 (green), and (G,H) virus capsids (red) and NPCs (green). Capsids, NPC, and lamin B1 were visualized with capsid protein, Nup153 and lamin B1 antibodies. Normalized correlative intensity profiles from yz cross-section close-ups are shown (C,F,I). Fluorescence line profile analysis of the intensity of capsids (red), NPCs (red/green) and lamin B1 (green) in a single optical section through the center of each nucleus are shown beside each image. Analysis was performed with ImageJ and Plot RGB Profile –plugin. Scale bars, 10 µm.

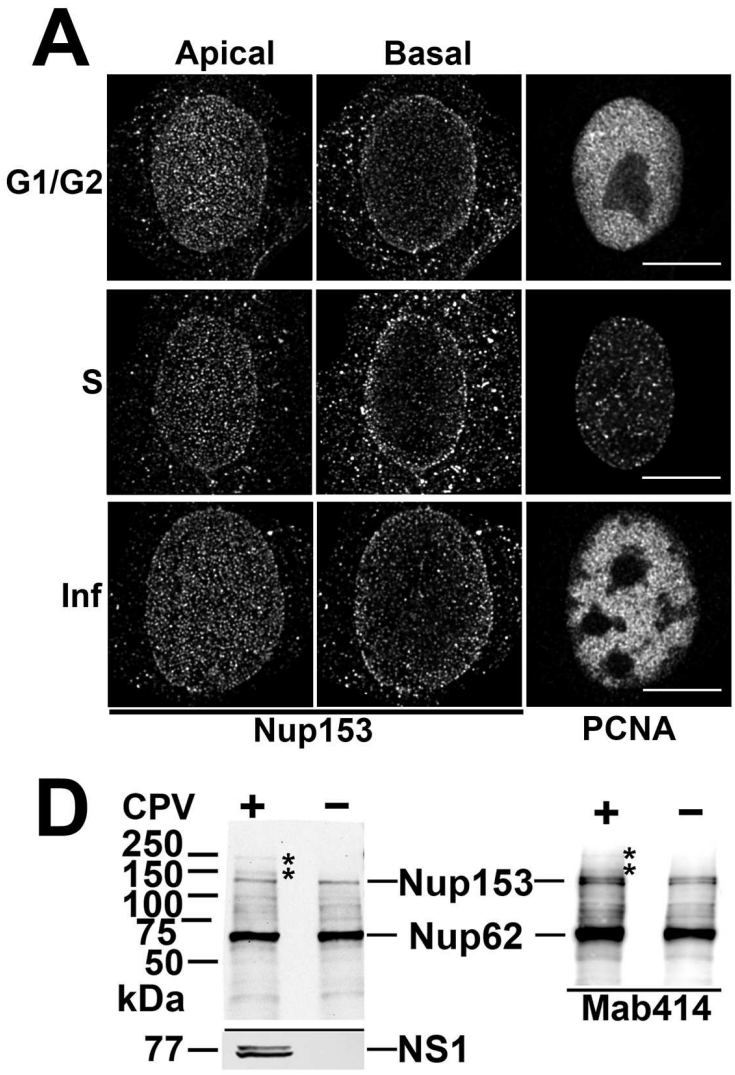

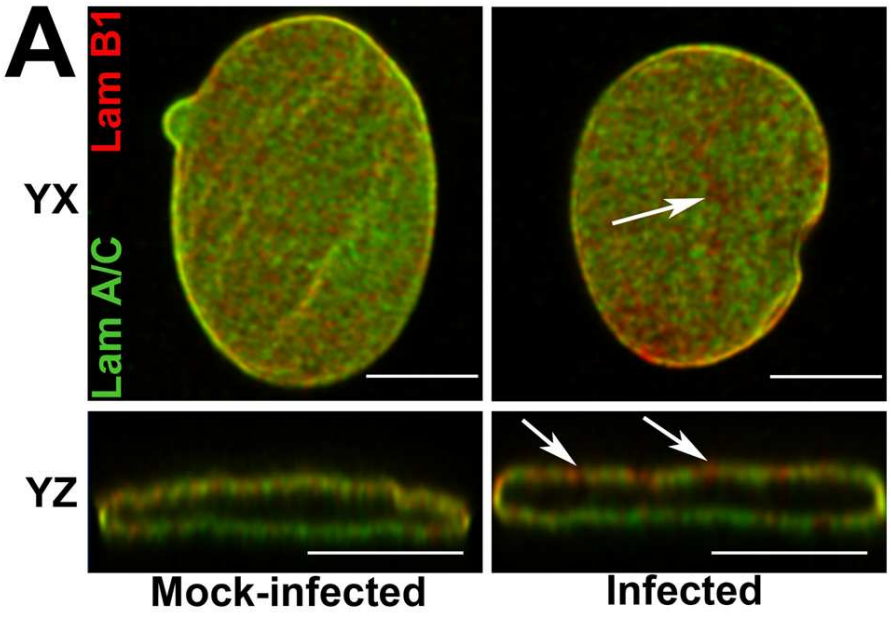

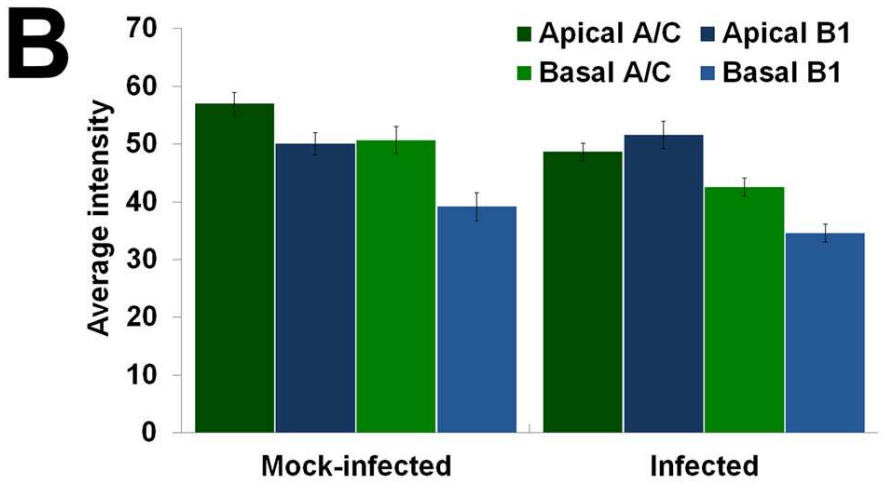

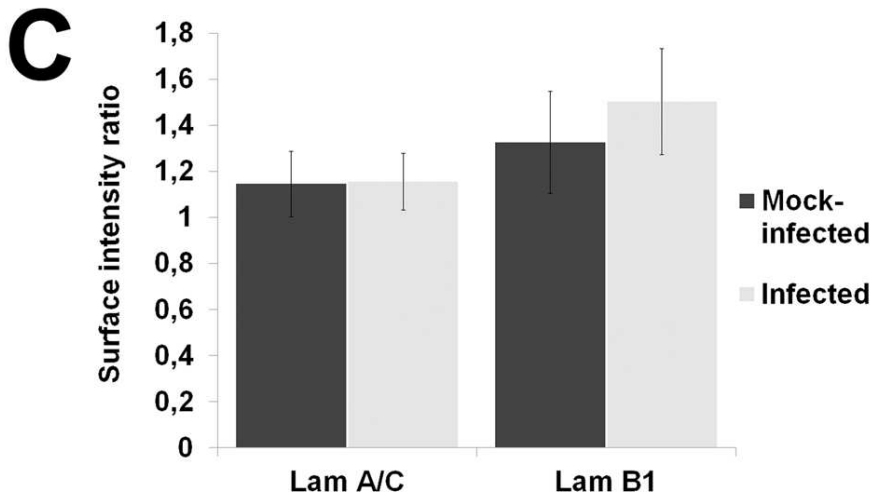

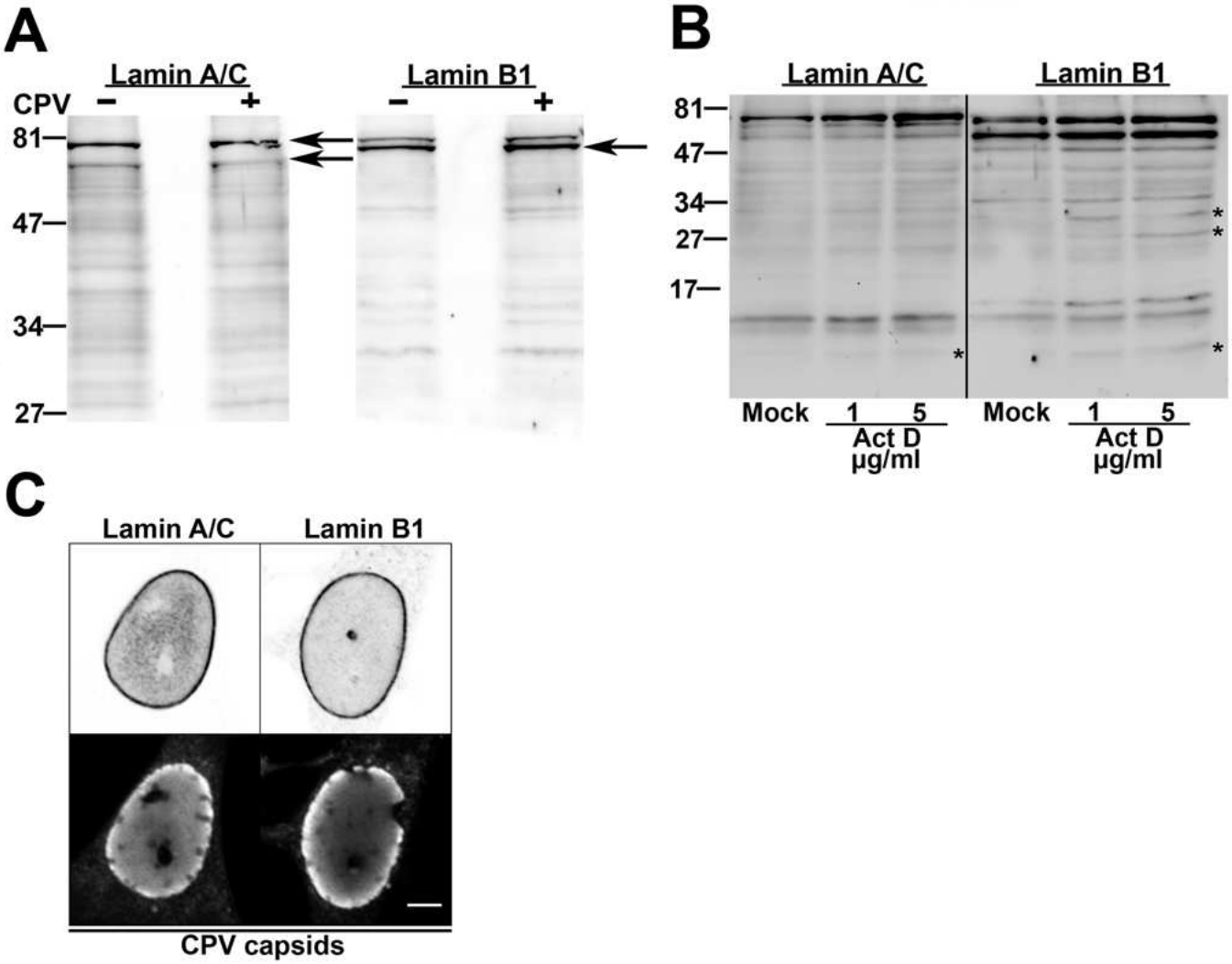

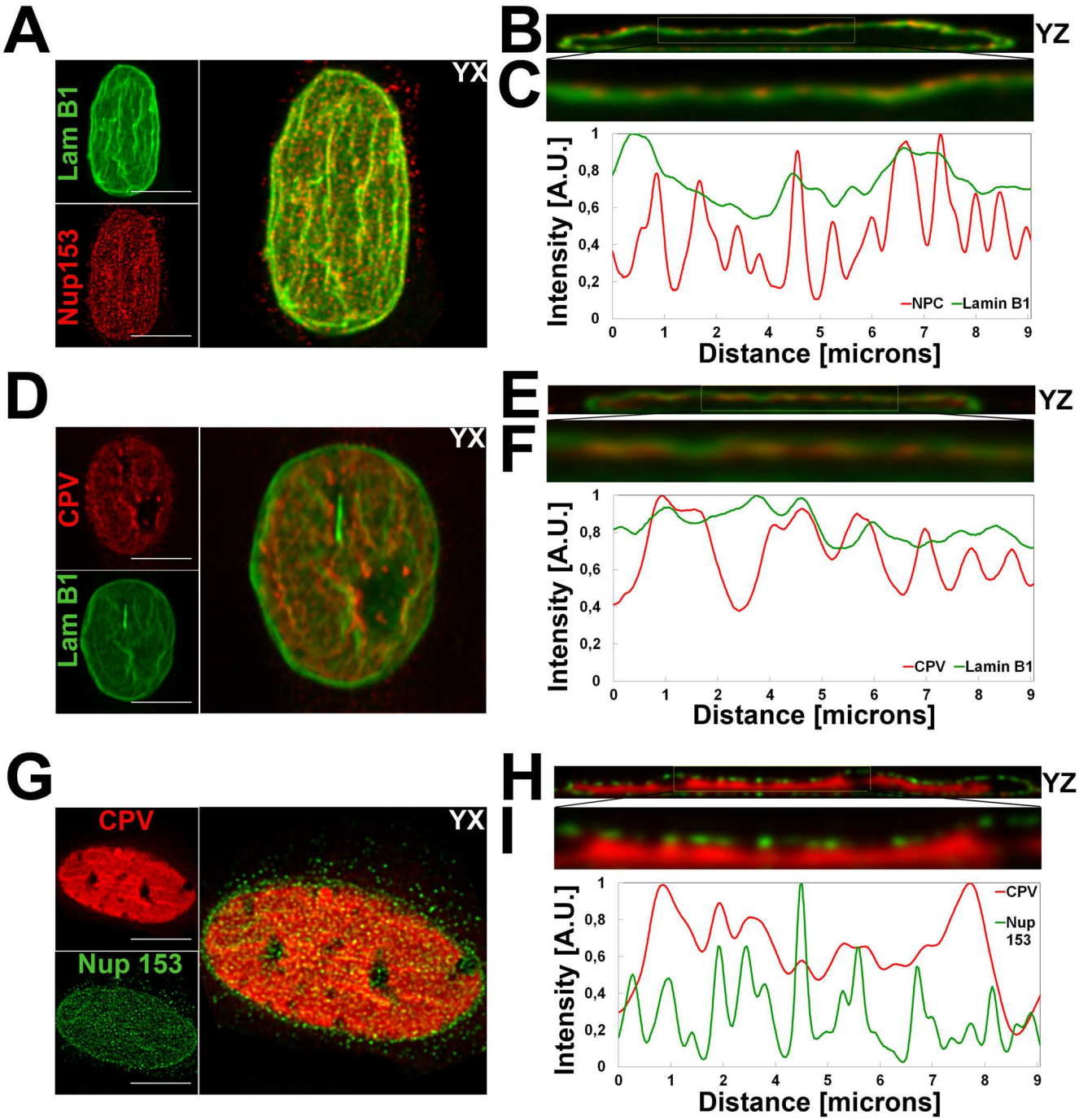

JVI Journal of Virology

Journal of Virology